NASA TECHNICAL NOTE

NASA TN D-4779

NASA TN D-4779

LIQUID DROPS: NUMERICAL AND ASYMPTOTIC SOLUTIONS OF THEIR SHAPES

by Kenneth J. Baumeister and Thomas D. Hamill

Lewis Research Center
Cleveland, Ohio

NATIONAL AERONAUTICS AND SPACE ADMINISTRATION • WASHINGTON, D. C. • SEPTEMBER 1968

NASA TN D-4779

LIQUID DROPS: NUMERICAL AND ASYMPTOTIC SOLUTIONS OF THEIR SHAPES

By Kenneth J. Baumeister and Thomas D. Hamill

Lewis Research Center
Cleveland, Ohio

NATIONAL AERONAUTICS AND SPACE ADMINISTRATION

For sale by the Clearinghouse for Federal Scientific and Technical Information
Springfield, Virginia 22151 – CFSTI price $3.00

ABSTRACT

The shapes of liquid drops resting on flat surfaces were determined by a Runge-Kutta solution of the Laplace capillary equation. A characteristic length equal to the square root of surface tension divided by the product of density and gravity was used to nondimensionalize the numerical results. In addition, asymptotic solutions for small and large drops were combined to give explicit expressions for the maximum drop height and radius. These correlations apply for the complete range of liquid volumes and contact angles.

LIQUID DROPS: NUMERICAL AND ASYMPTOTIC SOLUTIONS OF THEIR SHAPES

by Kenneth J. Baumeister and Thomas D. Hamill

Lewis Research Center

SUMMARY

The equilibrium shapes of liquid drops supported by a flat horizontal surface were determined as a function of the contact angle by solving the Laplace capillary equation. In addition, asymptotic solutions of the Laplace capillary equation for the case of large and small drops were combined to give explicit expressions for the maximum height and radius of the drop as a function of the contact angle for any liquid volume.

INTRODUCTION

The boiling and condensing heat-transfer characteristics of wetting and nonwetting liquids depends quite often on the geometrical characteristics of liquid drops in contact with solid surfaces. The contact areas are of particular importance in determining heat-transfer and vaporization rates.

For example, in the two-phase-mist-flow regime in the liquid-metal Rankine boiler, spiral inserts centrifuge entrained liquid droplets to the heated-tube wall. At the wall, the shape of the drop must be known if the vaporization characteristics are to be predicted. Poppendiek (ref. 1) has developed an analytical model for this flow based on a Leidenfrost boiling model. However, a complete analysis of Leidenfrost boiling requires a knowledge of the heat-transfer areas associated with a given size drop (ref. 2).

These facts provide the incentive for the present report, in which the equilibrium shapes of liquid drops supported by a flat horizontal surface are determined.

A liquid drop supported by a horizontal surface assumes a shape that depends on both molecular forces and body forces (gravity, etc.). For example, the photographs in figure 1 (taken from ref. 3) show the effect of gravity on a mercury drop resting on a surface. Clearly, the gravitational body force g will affect the energy transfer to the drop in a heating situation.

Molecular forces lead to the macroscopic phenomenon of surface tension. Since molecules are subjected to an unsymmetrical force field, the surface molecules are, in effect, pulled towards the interior of the liquid more strongly than towards the vapor. Complications arise because of the interaction between liquid molecules and the molecules of the solid supporting surfaces. These forces lead to the macroscopic phenomenon of contact angle, which is designated by θ in figure 2. The effect of surface attraction is pictured in this figure. However, from a macroscopic viewpoint, the shape of the drop is determined by gravity, surface tension, liquid density, and contact angle.

The mathematical formulation of the criterion of equilibrium of the drop surface is the Laplace capillary equation (ref. 4)

$$\frac{1}{R_1} + \frac{1}{R_2} = \frac{\Delta P}{\sigma} \tag{1}$$

where σ is the surface tension between the liquid and its vapor, R_1 and R_2 are the principle radii of curvature at any point on the drop surface as shown in figures 3 and 4, and ΔP is the pressure difference across the liquid interface at the point in question. Equation (1) can be derived from static equilibrium considerations (ref. 5) or by a variational technique of minimizing the total free energy of the drop (ref. 6). Equation (1) is rewritten in differential form by expressing the two radii of curvature in terms of differential notation.

Laplace, Gauss, Poisson, Gay-Lussac, and others (as cited in ref. 4) have attempted to solve equation (1). As yet, no general solution appears possible. The most complete work on this subject to date was by Bashforth and Adams (ref. 4). By suitable geometric transformations, Bashforth and Adams transformed equation (1) into a nonlinear second-order ordinary differential equation. This differential equation was then solved numerically by hand and the results tabulated in reference 4.

In their numerical solution of equation (1), Bashforth and Adams nondimensionalized the governing equation by introducing the radius of curvature of the drop at its apex as a characteristic length. However, for a given drop volume, the radius of curvature at the apex is not a known quantity. Consequently, as pointed out by Wark (ref. 7), parametric plots must be constructed from Bashforth and Adams tabulated results if the drop height and radius are to be explicitly related to the volume of a drop. This procedure proves to be inconvenient.

The characteristic length

$$\lambda = \sqrt{\frac{\sigma g_c}{\rho_L g}} \tag{2}$$

which is introduced in this report is more convenient to use since it depends only on the properties of the fluid and the gravitational field; whereas, Bashforth and Adams characteristic length depends on the shape of the drop. Because the characteristic length used in this report is different from that of reference 4, the numerical results were more easily obtained by a Runge-Kutta solution of equation (1) on a digital computer rather than attempting to use the tabulated results of reference 4. Also, the digital result has much greater accuracy.

Numerical solutions are presented for the maximum drop radius, drop height, and contact radius in terms of the drop volume for contact angles from 1^{o} to 180^{o}. In addition, asymptotic solutions of the Laplace capillary equation for the case of large and small drops are combined to give explicit expressions for the maximum height and radius of the drop as a function of the contact angle θ for any liquid volume V.

SYMBOLS

C	constant
g	acceleration of gravity, cm/sec^2
g_c	dimensional conversion factor, $(g)(cm)/(dynes)(sec^2)$ (pertains only to work done in English system of units)
h	height of drop, cm
$\bar{h}$	average height of drop
h^*	dimensionless height of drop, h/λ
$\bar{h}^*$	$\bar{h}/\lambda$
h_∞	maximum asymptotic (large drop) height of drop, cm
h_∞^*	dimensionless h_∞, h_∞/λ
j	$\sin \varphi$
ΔP	pressure drop across interface, $dynes/cm^2$ (N/cm^2)
R_o	radius of curvature of drop surface at apex of drop, cm
R_o^*	dimensionless R_o, R_o/λ
R_1, R_2	radii of curvature of drop surface, cm
R_1^*, R_2^*	dimensionless radii of curvature, R_1/λ and R_2/λ

r	maximum radius of drop, cm
r^*	dimensionless r, r/λ
r_c	surface contact radius, cm
r_c^*	dimensionless r_c, r_c/λ
r_∞	radius of drop associated with h_∞, cm
r_∞^*	dimensionless r_∞, r_∞/λ
S	unit of arc length, cm
S^*	dimensionless S, S/λ
V	volume of drop, cm^3
V^*	dimensionless V, V/λ^3
x	radial coordinate
x^*	dimensionless x, x/λ
Δx	numerical integration increment, cm
Δx^*	dimensionless Δx, $\Delta x/\lambda$
z	height coordinate, cm
z^*	dimensionless z, z/λ
z_o	z at apex of drop, cm
z_o^*	dimensionless z_o, z_o/λ
θ	contact angle, deg
λ	characteristic length (see eq. (2))
ρ_L	liquid density, g/cm^3
ρ_v	vapor density, g/cm^3
σ	surface tension, dynes/cm (N/cm)
φ	angle, deg (see fig. 4)

Subscripts:

i	numerical integration index
max	maximum

GOVERNING EQUATIONS

The solution of the Laplace capillary equation (eq. (1)) will determine the shape of the drop. This equation represents a force balance which relates the surface-tension forces and the pressure difference across the surface of a drop. At equilibrium the surface-tension forces must be balanced by the pressure difference across the free surface of the drop.

By expressing the pressure difference across the drop surface in terms of a liquid head and by introducing the characteristic length λ into equation (1), the governing equation becomes dimensionless and is of the form

$$\frac{1}{R_1^*} + \frac{1}{R_2^*} = z^* \tag{3}$$

(The starred quantities denote dimensionless terms.) The derivation of equation (3) is given in appendix A.

Equation (3) must, of course, be rewritten with the radii of curvature expressed in differential form before it can be solved directly. If R_1^* and R_2^* are expressed in terms of x^* and z^*, equation (3) can be transformed into a second-order nonlinear differential equation (see appendix A) of the form

$$\frac{d^2z^*}{dx^{*2}} + \frac{1}{x^*}\left[1 + \left(\frac{dz^*}{dx^*}\right)^2\right]\frac{dz^*}{dx^*} = \pm z^*\left[1 + \left(\frac{dz^*}{dx^*}\right)^2\right]^{3/2} \tag{4}$$

where x^* and z^* are the dimensionless coordinates of a point P on the drop surface (see fig. 4).

In principle, this differential equation must be solved to determine the shape of the drop. Since this equation cannot be solved explicitly, numerical procedures must be used. However, rather than a direct numerical attack on equation (4), reference 8 suggests the introduction of a new variable

$$j = \sin \varphi \tag{5}$$

as a means of simplifying the numerical work. When the new variable j is used, the Laplace capillary equation is transformed into a coupled pair of first-order differential equations (see appendix A). These equations are given by

$$\frac{dj}{dx^*} = z^* - \frac{j}{x^*} \tag{6}$$

$$\frac{dz^*}{dx^*} = \frac{j}{\pm\left(1 - j^2\right)^{1/2}} \tag{7}$$

Equations (6) and (7) represent the governing differential equations for the drop. These equations are solved by the Runge-Kutta method. (See appendix B for details of the numerical solution.)

DISCUSSION OF RESULTS

The numerical Runge solutions of the Laplace capillary equation are presented graphically in figures 5 to 9. Basically, for a given dimensionless drop volume and contact angle, these graphs enable the calculation of the following parameters:

(1) Maximum dimensionless height, h^*

(2) Maximum dimensionless drop radius, r^*

(3) Dimensionless contact radius, r_c^*

These three parameters, illustrated in figure 3, enable a sketch of the drop to be drawn and the contact areas to be determined. The numerical results from which these curves were plotted are given in table I.

Drop Height

In figures 5 and 6 the drop height h^* and $h^*/V^{*1/3}$, respectively, are plotted as a function of drop volume for various contact angles from 1° to 180°.

Any particular curve is characterized by two asymptotic regions. For very large volumes the drop height approaches a constant, the particular value of which depends on the contact angle. The second asymptote occurs for very small volumes. A very small drop assumes a spherical shape subject to the constraint imposed by a fixed contact angle. A completely nonwetting liquid ($\theta = 180^\circ$) forms a spherical drop in the limit as the volume approaches zero, while wetting liquids form truncated spheres in the zero volume limit. The two asymptotic regions are discussed quantitatively in the following paragraphs.

In the large-volume regime, a unique relation exists between the members of the family of curves. That is, the asymptotic height is given in terms of the contact angle by (ref. 9)

$$h_{\infty}^{*} \equiv \frac{h}{\sqrt{\frac{\sigma g_c}{\rho_L g}}} = \sqrt{2(1 - \cos\theta)} \tag{8}$$

This equation was derived by neglecting one of the radii of curvature in the Laplace equation. Equation (8) also predicts that the slope in the large-volume regime should be -3, since

$$\frac{h^*}{V^{*1/3}} = \frac{\sqrt{2(1 - \cos\theta)}}{V^{*1/3}} \tag{9}$$

or

$$\log V^* = 3 \log\left[\sqrt{2(1 - \cos\theta)}\right] - 3 \log\left(\frac{h^*}{V^{*1/3}}\right) \tag{10}$$

The equation allows the asymptotic thickness of a drop to be computed for arbitrary contact angle in the large-volume regime. As seen in figure 5, the large-volume regime is determined by $V^* > 100$.

The vertical asymptotes of figure 6 characterize the small-volume regime. Each contact angle gives a different asymptotic value for the dimensionless drop height, which can be computed from elementary geometric considerations. The equation for the dimensionless height in terms of the contact angle, derived in appendix C, is given by

$$\lim_{V^* \to 0} \frac{h^*}{V^{*1/3}} = \left[\frac{3(1 - \cos\theta)}{\pi(2 + \cos\theta)}\right]^{1/3} \tag{11}$$

The small-volume asymptotes derived numerically for various contact angles in figure 6 are identical to those predicted by equation (11), providing a further check on the accuracy of the numerical method. The plotted results of figure 6 indicate that a drop is "small" if $V^* < 0.01$, which serves as the criterion for the applicability of equation (11).

Drops whose volumes fall into the range $0.01 < V^* < 100$ are neither spherical nor pancaked in shape. No theoretical expression for the height of drops exists in this intermediate range. Based on the two asymptotic solutions, however, an empirical expression was deduced to fit the curves over the entire dimensionless volume range. The general correlation is given by

$$\frac{h^*}{h_\infty^*} = \left\{1 + \left[\frac{4\pi(2 + \cos\theta)\sin\frac{\theta}{2}}{3V^*}\right]^m\right\}^{-1/3m} \tag{12}$$

where m is an empirical constant chosen to fit the data in the intermediate range. The best choice of m is m = 1.0; this gave agreement to within 10 percent. Thus,

$$\frac{h^*}{h_\infty^*} = \left[\frac{3V^*}{3V^* + 4\pi(2 + \cos\theta)\sin\frac{\theta}{2}}\right]^{1/3} \tag{13}$$

The general correlation is compared graphically with exact numerical results in figure 7. The particular form of equation (12) was chosen, because irrespective of the choice of m this equation approaches equations (8) and (11) in the limit of very large and very small volumes, respectively.

Maximum Drop Radius

In figure 8 the dimensionless drop volume V^* is plotted against the dimensionless maximum radius r^*_{max} with contact angle θ as a parameter. These curves are also characterized by two asymptotic regions.

For large volumes,

$$V^* = \pi r_\infty^{*2} h_\infty^* \tag{14}$$

leading to a slope of 2 on a log-log paper, since h_∞^* remains constant in this range. Solving for r_∞^* in terms of volume and contact angle by employing the expression for h_∞^* (eq. (8)) gives

$$r_\infty^* = \left[\frac{V^*}{\pi\sqrt{2(1 - \cos\theta)}}\right]^{1/2} = \left(\frac{V^*}{\pi h_\infty^*}\right)^{1/2} \tag{15}$$

For very small volumes, geometrical considerations (see appendix C) lead to

$$V^* = \pi\left[(1 - \cos\theta)^2 - \frac{1}{3}(1 - \cos\theta)^3\right]R^{*3} \tag{16}$$

This equation gives a slope of 3 on log-log paper, as indicated by figure 8.

Solving for the radius of the sphere gives

$$R^* = \frac{V^{*1/3}}{\pi^{1/3}\left[(1 - \cos\theta)^2 - \frac{1}{3}(1 - \cos\theta)^3\right]^{1/3}} \tag{17}$$

For contact angles greater than 90^o, the radius of the sphere represents the maximum radius of the drop. However, for contact angles less than 90^o, the maximum drop radius r is given by

$$r^* = R^* \sin\theta = \frac{V^{*1/3}\sin\theta}{\pi^{1/3}\left[(1 - \cos\theta)^2 - \frac{1}{3}(1 - \cos\theta)^3\right]^{1/3}} \tag{18}$$

Now, the large- and small-drop results can be combined in the intermediate region between the two.

In the intermediate range there is a gradual change of slope in which the two asymptotic solutions blend into each other. There is no analytical expression for computing the maximum radius in the intermediate range. However, combining the two asymptotic solutions over the entire dimensionless volume range in the following manner gives, for $\theta < 90^o$,

$$\frac{r^*}{r^*_\infty} = \left(1 + \left\{\frac{\pi^{1/3}h^*_\infty \sin^2\theta}{V^{*1/3}\left[(1 - \cos\theta)^2 - \frac{1}{3}(1 - \cos\theta)^3\right]^{2/3}}\right\}^n\right)^{1/2n} \tag{19}$$

and for $\theta > 90^o$,

$$\frac{r^*}{r^*_\infty} = \left(1 + \left\{\frac{\pi^{1/3}h^*_\infty}{V^{*1/3}\left[(1 - \cos\theta)^2 - \frac{1}{3}(1 - \cos\theta)^3\right]^{2/3}}\right\}^n\right)^{1/2n} \tag{20}$$

A choice of $n = 1.8$ correlates the exact numerical results to within 2 percent. The agreement between the correlation and the exact numerical results is so close that no graphical comparison was made.

As before, the particular choice of the correlating equation is such that independent of the value of n the equation will converge to the proper asymptotic solution for the case of large and small drops.

Contact Radius

The contact radius r_c^*, which determines the area of physical contact between liquid and solid, is plotted against the maximum radius r^* in figure 9 for contact angles of 135° and 180°. For contact angles equal to or less than 90° the maximum radius equals the contact radius.

Average Drop Thickness

A parameter that has had some use in heat-transfer analysis is the average drop thickness $\bar{h}$ defined as

$$\bar{h}^* = \frac{V^*}{\pi r^{*2}} \tag{21}$$

and

$$\frac{\bar{h}^*}{V^{*1/3}} = \frac{V^{*2/3}}{\pi r^{*2}} \tag{22}$$

Both these quantities are listed in table I for various size drops.

Experimental Data

Some experimental data were available for various liquids, as indicated in figures 6 and 8, on the relation between volume and the maximum drop radius and height. The data given in reference 10 are for liquids in Leidenfrost film boiling, in which the liquid does not wet the surface. Consequently, the contact angle is 180°.

CONCLUDING REMARKS

Numerical solutions of the Laplace capillary equation were presented graphically for various contact angles. In addition, the generalized correlating equations for the maximum thickness and radius of a drop for arbitrary drop volume and contact angle were synthesized by combining the asymptotic solutions for very large and very small drops. These correlation equations are accurate to within 10 percent on drop height and 2 percent on maximum drop radius.

Lewis Research Center,
National Aeronautics and Space Administration,
Cleveland, Ohio, May 22, 1968,
129-01-11-02-22.

APPENDIX A

TRANSFORMATION OF LAPLACE'S CAPILLARY EQUATION

The governing equation for the shape of the drop, Laplace's equation, is given by equation (1) (repeated here for convenience).

$$\frac{1}{R_1} + \frac{1}{R_2} = \frac{\Delta P}{\sigma} \tag{A1}$$

The pressure difference across the drop is proportional to the sum of the reciprocal of the radii of curvature in two mutually perpendicular directions, as depicted in figure 4. Note in equation (A1) that the expression

$$\frac{1}{R_1} + \frac{1}{R_2}$$

is an invariant with respect to the coordinate system chosen.

The pressure difference ΔP in equation (A1) is a function of z which can be conveniently expressed as

$$\Delta P = \rho_L (z - z_o) \frac{g}{g_c} + C \tag{A2}$$

where the vapor density ρ_v is assumed much less than ρ_L and the constant C represents the jump in pressure across the liquid-liquid interface at $z = z_o$ and $x = 0$ (the top of the drop).

At the top of the drop, the radii of curvature are equal; thus, Laplace's capillary equation (eq. (A1)) becomes

$$\Delta P \Big|_{\substack{z=z_o \\ x=0}} = \frac{2\sigma}{R_o} = C \tag{A3}$$

where R_o is the radius of curvature at the top of the drop. Substituting equation (A3) into the expression for ΔP (e.g., eq. (A2)) gives

$$\Delta P = \rho_L z \frac{g}{g_c} + \frac{2\sigma}{R_o} - z_o \frac{g}{g_c} \rho_L \tag{A4}$$

Up to this time, the quantity z_o represented an arbitrary distance from the reference coordinate to the top of the drop. However, z_o is now taken as

$$z_o = \frac{2\sigma}{R_o} \frac{g_c}{\rho_L g} \tag{A5}$$

Substituting this expression into equation (A4) gives

$$\Delta P = \rho_L z \frac{g}{g_c} \tag{A6}$$

Thus, the governing equation (eq. (A1)) becomes, by substituting equation (A6) into equation (A1),

$$\frac{1}{R_1} + \frac{1}{R_2} = \frac{\rho_L z \frac{g}{g_c}}{\sigma} \tag{A7}$$

The radius of curvature at the top of the drop R_o can now be written from equation (A5) as

$$R_o = \frac{2\sigma}{\rho_L z_o \frac{g}{g_c}} \tag{A8}$$

The parameter z_o is considered an independent variable which can be chosen arbitrarily to give various radii of curvature at the top of the drop.

Choosing z_o as the independent variable, the volume of the drop becomes a dependent variable, that is

$$V = f(z_o) \tag{A9}$$

The functional form in equation (A9) cannot be determined explicitly, rather it can be represented in a geometrical fashion from the numerical solution of equation (A1).

The governing equations have been discussed briefly and now will be transformed to a more convenient form for solution.

Dividing both sides of the governing equation (A7) by the characteristic length λ (defined by eq. (2)) yields

$$\frac{1}{R_1^*} + \frac{1}{R_2^*} = z^* \tag{A10}$$

where

$$\left.\begin{aligned} R_1^* &= \frac{R_1}{\lambda} \\ R_2^* &= \frac{R_2}{\lambda} \end{aligned}\right\} \tag{A11}$$

and

$$z^* = \frac{z}{\lambda} \tag{A12}$$

(The starred symbols represent dimensionless coordinates.)

The dimensionless Laplace capillary equation given by equation (A10) can now be written in terms of dimensionless variables x^* and the angle φ (see fig. 4).

Consider the point P on the surface of the drop defined by the coordinates φ and x^*. The radii of curvature R_1^* at the general point P can now be represented from geometrical considerations (see fig. 4)

$$R_2^* = \frac{x^*}{\sin \varphi} = \frac{x^*}{j} \tag{A13}$$

The radius of curvature R_2^* must intersect the $x^* = 0$ line because of the symmetrical nature of the drop.

Similarly, the radius of curvature R_1^* can be expressed in terms of x^* and φ by considering the distance traveled along an elemental length change dS^*. Mathematically,

$$dS^* = R_1^* \, d\varphi \tag{A14}$$

However, the arc dS^* is perpendicular to the arc traversed by R_2^*; thus, from geometrical considerations

$$dx^* = \cos \varphi \, dS^* \tag{A15}$$

Combining equations (A14) and (A15) and eliminating dS^* yields

$$\frac{1}{R_1^*} = \cos\varphi \frac{d\varphi}{dx^*} = \frac{d \sin\varphi}{dx^*} \tag{A16}$$

Substituting the values of R_1^* and R_2^* from equations (A13) and (A16) into the governing equation (eq. (A10)) yields

$$\frac{d \sin\varphi}{dx^*} + \frac{\sin\varphi}{x^*} = z^* \tag{A17}$$

However, $\sin\varphi$ can be expressed in terms of the variables z^* and x^* by noting that

$$\frac{dz^*}{dx^*} = \tan\varphi = \frac{\sin\varphi}{\pm\sqrt{1 - \sin^2\varphi}} \tag{A18}$$

and

$$\sin\varphi = \frac{\tan\varphi}{\pm\sqrt{1 + \tan^2\varphi}} \tag{A19}$$

The sign is determined by the quadrant in which the integration occurs.

Eliminating $\sin\varphi$ from governing equation (A17) by use of equation (A19) and replacing $\tan\varphi$ by dz^*/dx^* from equation (A18) yield

$$\frac{d^2z^*}{dx^{*2}} + \frac{1}{x^*}\left[1 + \left(\frac{dz^*}{dx^*}\right)^2\right]\frac{dz^*}{dx^*} = \pm z^*\left[1 + \left(\frac{dz^*}{dx^*}\right)^2\right]^{3/2} \tag{A20}$$

This is the basic governing differential equation for the shape of a drop. The equation is a second-order nonlinear differential equation which, up to the present time, has not been solved explicitly.

Bashforth and Adams (ref. 4) solved the same type of equation by a direct numerical assault. However, Timoshenko and Woinowsky-Krieger (ref. 8) suggest the introduction of the new variable

$$j = \sin\varphi \tag{A21}$$

as a simpler approach to solving the problem.

Substituting the new variable j (eq. (A21)) into equations (A17) and (A18) yields

$$\frac{dj}{dx^*} + \frac{j}{x^*} = z^* \tag{A22}$$

$$\frac{dz^*}{dx^*} = \frac{j}{\pm\left(1 - j^2\right)^{1/2}} \tag{A23}$$

Thus, the second-order governing equation (A20) has been transformed into two first-order differential equations which are much simpler to handle mathematically. These equations are equations (6) and (7) in the main text.

APPENDIX B

NUMERICAL PROCEDURES

The numerical procedures used in solving the governing equations (6) and (7) are described briefly. These equations are solved by a double-precision fourth-order Runge-Kutta numerical integration. The numerical procedure for solving two simultaneous first-order differential equations by the Runge-Kutta method is given in most texts in numerical analysis and need not be discussed herein. However, there are a few salient points that will be considered.

Increment Size

The increment size for the various drop volumes was chosen to be sufficiently small such that in most cases the results are accurate to three significant figures. This accuracy was accomplished by iteration using ever smaller values of Δx. The values of Δx chosen are listed in table I along with the numerical results.

To increase the accuracy of the integration in the region where φ equals 90°, Δx was reduced by a factor of 100 (0.01 Δx) for $85^{\circ} < \varphi < 95^{\circ}$.

Initial Conditions on z_0^*

At the top of the drop, principle radii of curvature become equal because of symmetry. Consequently, at the top of the drop the governing equation (eq. (3)) takes the form

$$R_0^* = \frac{2}{z_0^*} \tag{B1}$$

where o denotes the apex position of the drop. At the start of the numerical integration, the position of the apex of the drop is chosen arbitrarily at some value of z_0^* (fig. 3). By choosing z_0^* as an initial condition of the solution, the radius R_0^* and the volume of the drop will be uniquely determined. Thus, the drop volume becomes a dependent variable.

If z_0^* is initially chosen to be small, the radius of curvature at the apex of the drop becomes large (see eq. (B1)). The drop takes on a pancake or disk-like shape. If z_0^* is initially chosen to be large, R_0^* becomes small, and the drop takes on a spherical shape. By choosing numerous numerical values of z_0^* and solving each problem, the

shape of the drop can be found for various values of V (see eq. (A9)).

In addition, it should be noted that the Runge-Kutta technique puts an upper limit on the choice of Δx, in that at the initial starting point,

$$\Delta x^* < \frac{4}{z_o^*} \tag{B2}$$

in order to prevent the occurrence of imaginary numbers resulting from the denominator in equation (7).

Thus, for large initial choices of z_o consideration must be given to the choice of Δx^*.

Tan φ

The differential dz^*/dx^* in equation (7) equals $\tan \varphi$. Consequently, for $\varphi < 90^o$ the $\tan \varphi$ is positive while for $\varphi > 90^o$, $\tan \varphi$ is negative. Thus, a $\pm$ sign is displayed in equation (7) to indicate that a sign change is required during the numerical integration.

Initial Conditions

From the choice of coordinates shown in figure 2, the initial conditions for this problem are

$$x^* = 0 \qquad z^* = z_o^* \tag{B3}$$

$$x^* = 0 \text{ (or } j = 0) \qquad \frac{dz^*}{dx^*} = 0 \tag{B4}$$

$$x^* = 0 \qquad \frac{j}{x} = \frac{z_o^*}{2} \tag{B5}$$

Initial condition (B5) comes directly from combining equation (A13) with equation (B1) at the apex of the drop.

Drop Volume

Since the solution of the governing equations requires numerical integration, the numerical results will be a set of ordered numbers z_i^*, x_i^* which describe the shape of the drop. The dimensionless volume V^* is computed by using the trapezoidal rule as

$$V^* = \frac{\pi}{3} \sum_{i=1}^{n} \left(z_i^* - z_{i-1}^*\right)\left(x_i^{*2} + x_{i-1}^{*2} + x_i^* x_{i-1}^*\right) \tag{B6}$$

where n represents the total number of numerical steps in the integration.

APPENDIX C

GEOMETRICAL RELATION FOR SPHERICAL DROPS

The volume of a truncated sphere (often called a spherical segment) is given by

$$V = \frac{\pi}{3} h^2(3R - h) \tag{C1}$$

(see fig. 10) where h is the vertical distance from the plate to the apex of the spherical drop and R is the radius of the sphere. From geometry a unique relation exists among R, h, and the contact angle θ; thus,

$$R = \frac{h}{(1 - \cos\theta)} \tag{C2}$$

Substituting equation (C2) into equation (C1) and rearranging gives

$$\frac{h}{V^{1/3}} = \frac{h^*}{V^{*1/3}} = \frac{1}{\left[\pi\left(\frac{1}{1 - \cos\theta} - \frac{1}{3}\right)\right]^{1/3}} \tag{C3}$$

or

$$\frac{h^*}{V^{*1/3}} = \left[\frac{3(1 - \cos\theta)}{\pi(2 + \cos\theta)}\right]^{1/3} \tag{C4}$$

This relation is valid for all contact angles.

Combining equations (C2) and (C3) gives for the radius of a sphere

$$R^* = \frac{V^{*1/3}}{\pi^{1/3}\left[(1 - \cos\theta)^2 - \frac{1}{3}(1 - \cos\theta)^3\right]^{1/3}} \tag{C5}$$

REFERENCES

1. Poppendiek, H. F., et al.: High Acceleration Field Heat Transfer for Auxiliary Space Nuclear Power Systems. Rep. SAN-409-29, Geoscience Ltd., Jan. 1966.
2. Baumeister, Kenneth J.; Hamill, Thomas D.; and Schoessow, Glenn J.: A Generalized Correlation of Vaporization Times of Drops in Film Boiling on a Flat Plate. Proceedings of the Third International Heat Transfer Conference, Chicago, Ill., Aug. 7-12, 1966. Vol. 4, AIChE, 1966, pp. 66-73.
3. Sturas, Jonas I.; Crabs, Clifford C.; and Gorland, Sol H.: Photographic Study of Mercury Droplet Parameters Including Effects of Gravity. NASA TN D-3705, 1966.
4. Bashforth, Francis: An Attempt to Test the Theories of Capillary Action by Comparing the Theoretical and Measured Forms of Drops of Fluid. Cambridge Univ. Press, 1883.
5. Prandtl, L.; and Tietjens, O. G. (L. Rosenhead, trans.): Fundamentals of Hydro- and Aeromechanics. Dover Publications, 1957.
6. Landau, Lev D.; and Lifshitz, E. M.: Fluid Mechanics. Addison-Wesley Pub. Co., Inc., 1959.
7. Wark, Ian W.: The Physical Chemistry of Flotation. I. The Significance of Contact Angle in Flotation. J. Phys. Chem., vol. 37, no. 5, May 1933, pp. 623-644.
8. Timoshenko, Stephen P.; and Woinowsky-Krieger, S.: Theory of Plates and Shells. Second ed., McGraw-Hill Book Co., Inc., 1959.
9. Adamson, Arthur W.; and Ling, Irene: The Status of Contact Angle as a Thermodynamic Property. Advances in Chemistry Series 43, Contact Angle, Wettability, and Adhesion. American Chemical Society, 1964.
10. Borishansky, V. M.: Heat Transfer to a Liquid Freely Flowing Over a Surface Heated to a Temperature Above the Boiling Point. Problems of Heat Transfer During a Change of State: A Collection of Articles. S. S. Kutateladze, ed. AEC-tr-3405, 1953.

TABLE I. - NUMERICAL VALUES OF DROP SHAPE

$\sin\theta$	V^*	r^*	h^*	$h^*/V^{*1/3}$
		z_o = 0.4E 02; Δx = 0.1E-05		
0.17460E-01	0.912E-11	0.873E-03	0.762E-05	0.365E-01
0.87160E-01	0.568E-08	0.436E-02	0.190E-03	0.107E 00
0.25883E 00	0.451E-06	0.129E-01	0.170E-02	0.222E 00
0.42262E 00	0.334E-05	0.211E-01	0.468E-02	0.313E 00
0.70712E 00	0.304E-04	0.354E-01	0.146E-01	0.469E 00
0.10000E 01	0.261E-03	0.500E-01	0.499E-01	0.781E 00
0.70709E 00	0.492E-03	0.354E-01	0.851E-01	0.108E 01
-0.26043E-04	0.522E-03	0.205E-02	0.996E-01	0.124E 01
$\bar{h}$ = 0.665E-01		$\bar{h}/V^{*1/3}$ = 0.826		
		z_o = 0.1E 02; Δx = 0.1E-04		
0.17500E-01	0.589E-09	0.350E-02	0.306E-04	0.365E-01
0.87203E-01	0.364E-06	0.174E-01	0.762E-03	0.107E 00
0.25884E 00	0.288E-04	0.518E-01	0.681E-02	0.222E 00
0.42264E 00	0.213E-03	0.844E-01	0.187E-01	0.313E 00
0.70714E 00	0.193E-02	0.141E 00	0.583E-01	0.469E 00
0.10000E 01	0.163E-01	0.199E 00	0.197E 00	0.777E 00
0.70711E 00	0.303E-01	0.143E 00	0.331E 00	0.106E 01
-0.10494E-04	0.322E-01	0.314E-01	0.382E 00	0.120E 01
$\bar{h}$ = 0.260E 00		$\bar{h}/V^{*1/3}$ = 0.816		
		z_o = 0.4E 01; Δx = 0.1E-04		
0.17460E-01	0.912E-08	0.873E-02	0.762E-04	0.365E-01
0.87161E-01	0.568E-05	0.436E-01	0.190E-02	0.107E 00
0.25882E 00	0.448E-03	0.129E 00	0.170E-01	0.222E 00
0.42264E 00	0.328E-02	0.210E 00	0.464E-01	0.313E 00
0.70711E 00	0.287E-01	0.348E 00	0.143E 00	0.466E 00
0.10000E 01	0.222E 00	0.481E 00	0.458E 00	0.757E 00
0.70709E 00	0.396E 00	0.371E 00	0.734E 00	0.100E 01
-0.24069E-04	0.424E 00	0.167E 00	0.827E 00	0.110E 01
$\bar{h}$ = 0.582E 00		$\bar{h}/V^{*1/3}$ = 0.775		
		z_o = 0.1E 01; Δx = 0.1E-03		
0.17453E-01	0.583E-06	0.349E-01	0.305E-03	0.365E-01
0.87178E-01	0.359E-03	0.174E 00	0.757E-02	0.106E 00
0.25886E 00	0.260E-01	0.502E 00	0.650E-01	0.219E 00
0.42265E 00	0.165E 00	0.782E 00	0.166E 00	0.304E 00
0.70711E 00	0.104E 01	0.116E 01	0.439E 00	0.433E 00
0.10000E 01	0.484E 01	0.147E 01	0.108E 01	0.636E 00
0.70710E 00	0.755E 01	0.130E 01	0.151E 01	0.767E 00
-0.21354E-03	0.816E 01	0.992E 00	0.164E 01	0.815E 00
$\bar{h}$ = 0.121E 01		$\bar{h}/V^{*1/3}$ = 0.599		

TABLE I. - Continued. NUMERICAL VALUES OF DROP SHAPE

sin θ	V*	r*	h*	$h^*/V^{*1/3}$

z_o = 0.4E 00; Δx = 0.1E-03

0.17457E-01	0.909E-05	0.872E-01	0.761E-03	0.365E-01
0.87171E-01	0.527E-02	0.426E 00	0.184E-01	0.106E 00
0.25885E 00	0.271E 00	0.111E 01	0.136E 00	0.210E 00
0.42263E 00	0.123E 01	0.157E 01	0.299E 00	0.279E 00
0.70711E 00	0.505E 01	0.208E 01	0.549E 00	0.378E 00
0.10000E 01	0.167E 02	0.241E 01	0.135E 01	0.527E 00
0.70710E 00	0.245E 02	0.223E 01	0.179E 01	0.618E 00
-0.22743E-03	0.265E 02	0.190E 01	0.194E 01	0.650E 00

$\bar{h}$ = 0.146E 01 $\bar{h}/V^{*1/3}$ = 0.488

z_o = 0.1E 00; Δx = 0.1E-03

0.17456E-01	0.555E-03	0.344E 00	0.298E-02	0.363E-01
0.87156E-01	0.169E 00	0.138E 01	0.540E-01	0.977E-01
0.25883E 00	0.269E 01	0.253E 01	0.239E 00	0.172E 00
0.42262E 00	0.745E 01	0.306E 01	0.429E 00	0.220E 00
0.70712E 00	0.205E 02	0.360E 01	0.795E 00	0.291E 00
0.10000E 01	0.526E 02	0.393E 01	0.149E 01	0.399E 00
0.70702E 00	0.736E 02	0.375E 01	0.194E 01	0.463E 00
-0.19288E-03	0.798E 02	0.341E 01	0.209E 01	0.485E 00

$\bar{h}$ = 0.165E 01 $\bar{h}/V^{*1/3}$ = 0.382

z_o = 0.4E-01; Δx = 0.1E-03

0.17452E-01	0.698E-02	0.806E 00	0.676E-02	0.354E-01
0.87158E-01	0.730E 00	0.234E 01	0.768E-01	0.853E-01
0.25884E 00	0.642E 01	0.354E 01	0.269E 00	0.145E 00
0.42264E 00	0.152E 02	0.407E 01	0.458E 00	0.185E 00
0.70717E 00	0.370E 02	0.461E 01	0.821E 00	0.246E 00
0.10000E 01	0.875E 02	0.493E 01	0.151E 01	0.340E 00
0.70704E 00	0.121E 03	0.476E 01	0.196E 01	0.396E 00
-0.12740E-03	0.131E 03	0.441E 01	0.211E 01	0.415E 00

$\bar{h}$ = 0.171E 01 $\bar{h}/V^{*1/3}$ = 0.337

z_o = 0.1E-01; Δx = 0.1E-02

0.17455E-01	0.109E 00	0.210E 01	0.145E-01	0.303E-01
0.87176E-01	0.267E 01	0.387E 01	0.916E-01	0.660E-01
0.25886E 00	0.152E 02	0.506E 01	0.282E 00	0.114E 00
0.42286E 00	0.320E 02	0.558E 01	0.468E 00	0.147E 00
0.70713E 00	0.707E 02	0.611E 01	0.824E 00	0.199E 00
0.99999E 00	0.156E 03	0.643E 01	0.150E 01	0.279E 00
0.70536E 00	0.213E 03	0.625E 01	0.195E 01	0.326E 00
-0.67963E-03	0.230E 03	0.590E 01	0.210E 01	0.342E 00

$\bar{h}$ = 0.177E 01 $\bar{h}/V^{*1/3}$ = 0.289

TABLE I. - Continued. NUMERICAL VALUES OF DROP SHAPE

$\sin\theta$	V^*	r^*	h^*	$h^*/V^{*1/3}$
		z_o = 0.4E-02; Δx = 0.1E-02		
0.17462E-01	0.308E 00	0.311E 01	0.174E-01	0.257E-01
0.87228E-01	0.466E 01	0.488E 01	0.940E-01	0.563E-01
0.25898E 00	0.231E 02	0.605E 01	0.282E 00	0.990E-01
0.42270E 00	0.463E 02	0.657E 01	0.466E 00	0.130E 00
0.70716E 00	0.986E 02	0.709E 01	0.819E 00	0.177E 00
0.99999E 00	0.212E 03	0.741E 01	0.150E 01	0.251E 00
0.70676E 00	0.287E 03	0.723E 01	0.194E 01	0.294E 00
-0.48775E-03	0.311E 03	0.688E 01	0.209E 01	0.308E 00
$\bar{h}$ = 0.180E 01		$\bar{h}/V^{*1/3}$ = 0.256		
		z_o = 0.1E-02; Δx = 0.1E-02		
0.17460E-01	0.826E 00	0.464E 01	0.187E-01	0.200E-01
0.87182E-01	0.865E 01	0.638E 01	0.941E-01	0.458E-01
0.25890E 00	0.377E 02	0.753E 01	0.279E 00	0.833E-01
0.42290E 00	0.727E 02	0.805E 01	0.462E 00	0.111E 00
0.70753E 00	0.149E 03	0.856E 01	0.812E 00	0.153E 00
0.10000E 01	0.312E 03	0.888E 01	0.148E 01	0.219E 00
0.70581E 00	0.419E 03	0.870E 01	0.192E 01	0.257E 00
-0.14043E-02	0.454E 03	0.835E 01	0.207E 01	0.270E 00
$\bar{h}$ = 0.184E 01		$\bar{h}/V^{*1/3}$ = 0.239		
		z_o = 0.1E-03; Δx = 0.1E-02		
0.17463E-01	0.222E 01	0.712E 01	0.187E-01	0.144E-01
0.87192E-01	0.178E 02	0.882E 01	0.926E-01	0.354E-01
0.25901E 00	0.697E 02	0.996E 01	0.275E 00	0.669E-01
0.42281E 00	0.129E 03	0.105E 02	0.455E 00	0.901E-01
0.70778E 00	0.255E 03	0.110E 02	0.802E 00	0.126E 00
0.99999E 00	0.517E 03	0.113E 02	0.147E 01	0.183E 00
0.70530E 00	0.691E 03	0.111E 02	0.191E 01	0.216E 00
-0.71106E-03	0.748E 03	0.108E 02	0.206E 01	0.227E 00
$\bar{h}$ = 0.187E 01		$\bar{h}/V^{*1/3}$ = 0.206		
		z_o = 0.1E-05; Δx = 0.1E-02		
0.17457E-01	0.688E 01	0.120E 02	0.182E-01	0.959E-02
0.87192E-01	0.454E 02	0.136E 02	0.907E-01	0.254E-01
0.25898E 00	0.161E 03	0.148E 02	0.271E 00	0.497E-01
0.42270E 00	0.287E 03	0.152E 02	0.448E 00	0.679E-01
0.70768E 00	0.547E 03	0.158E 02	0.791E 00	0.967E-01
0.10000E 01	0.108E 04	0.161E 02	0.145E 01	0.142E 00
0.70600E 00	0.143E 04	0.159E 02	0.189E 01	0.168E 00
-0.14109E-02	0.155E 04	0.155E 02	0.204E 01	0.176E 00
$\bar{h}$ = 0.191E 01		$\bar{h}/V^{*1/3}$ = 0.165		

TABLE I. - Concluded. NUMERICAL VALUES OF DROP SHAPE

$\sin\theta$	V^*	r^*	h^*	$h^*/V^{*1/3}$
		z_o = 0.1E-07; Δx = 0.1E-02		
0.17455E-01	0.140E 02	0.167E 02	0.180E-01	0.747E-02
0.87192E-01	0.851E 02	0.184E 02	0.893E-01	0.204E-01
0.25901E 00	0.288E 03	0.195E 02	0.268E 00	0.406E-01
0.42299E 00	0.504E 03	0.200E 02	0.444E 00	0.558E-01
0.70769E 00	0.944E 03	0.205E 02	0.785E 00	0.800E-01
0.99999E 00	0.183E 04	0.208E 02	0.144E 01	0.118E 00
0.70603E 00	0.242E 04	0.206E 02	0.188E 01	0.140E 00
-0.86892E-03	0.262E 04	0.203E 02	0.203E 01	0.147E 00
$\bar{h}$ = 0.193E 01		$\bar{h}/V^{*1/3}$ = 0.140		
		z_o = 0.1E-09; Δx = 0.1E-02		
0.17466E-01	0.235E 02	0.214E 02	0.179E-01	0.625E-02
0.87194E-01	0.137E 03	0.231E 02	0.892E-01	0.173E-01
0.25888E 00	0.451E 03	0.242E 02	0.267E 00	0.348E-01
0.42288E 00	0.781E 03	0.247E 02	0.442E 00	0.480E-01
0.70755E 00	0.145E 04	0.252E 02	0.781E 00	0.691E-01
0.99999E 00	0.277E 04	0.255E 02	0.144E 01	0.102E 00
0.70580E 00	0.366E 04	0.253E 02	0.187E 01	0.121E 00
-0.19854E-02	0.396E 04	0.250E 02	0.202E 01	0.128E 00
$\bar{h}$ = 0.194E 01		$\bar{h}/V^{*1/3}$ = 0.123		
		z_o = 0.1E-12; Δx = 0.1E-02		
0.17462E-01	0.422E 02	0.285E 02	0.178E-01	0.511E-02
0.87209E-01	0.237E 03	0.301E 02	0.888E-01	0.144E-01
0.25895E 00	0.763E 03	0.312E 02	0.265E 00	0.291E-01
0.42263E 00	0.131E 04	0.317E 02	0.440E 00	0.402E-01
0.70783E 00	0.239E 04	0.322E 02	0.778E 00	0.582E-01
0.99999E 00	0.455E 04	0.325E 02	0.143E 01	0.863E-01
0.70552E 00	0.599E 04	0.323E 02	0.186E 01	0.103E 00
-0.12490E-02	0.648E 04	0.320E 02	0.202E 01	0.108E 00
$\bar{h}$ = 0.195E 01		$\bar{h}/V^{*1/3}$ = 0.105		

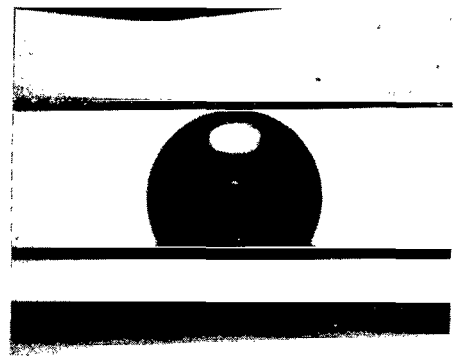

(a) Zero gravity.

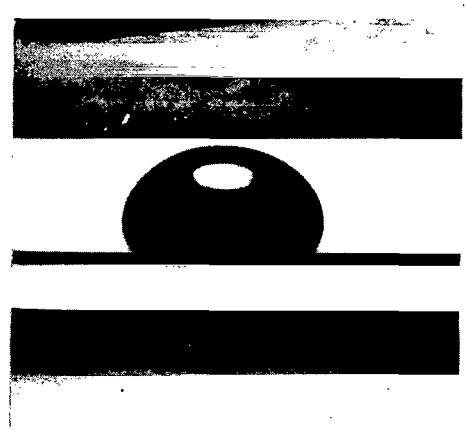

(b) 1 g.

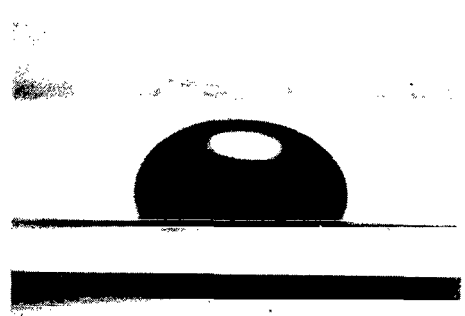

C-66-3242

(c) $1\frac{1}{2}$ g's.

Figure 1. - Variation of mercury droplet shape with gravity level. (Ref. 3)

(a) Wetting drop, $0° < \theta < 90°$.

(b) Intermediate case, $\theta = 90°$.

(c) Nonwetting drop, $90° < \theta < 180°$.

(d) No surface attraction.

Figure 2. - Drops resting on flat surface, shown in order of decreasing molecular attraction between liquid and solid.

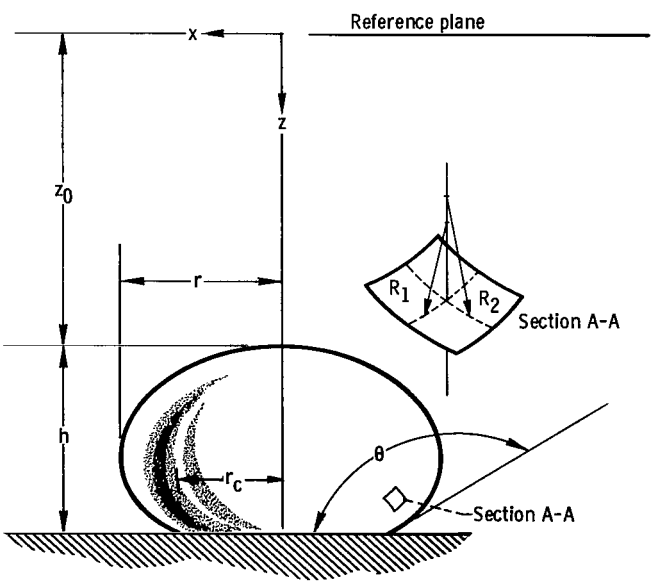

Figure 3. - Drop schematic.

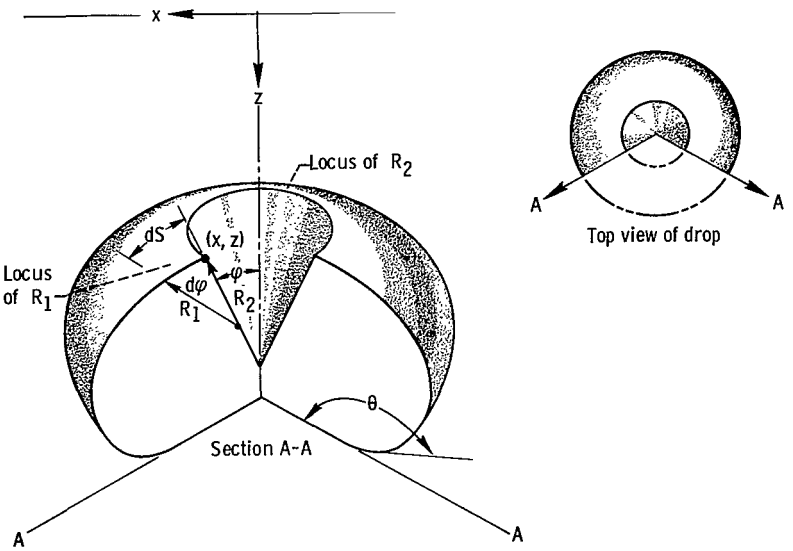

Figure 4. - Drop cross section.

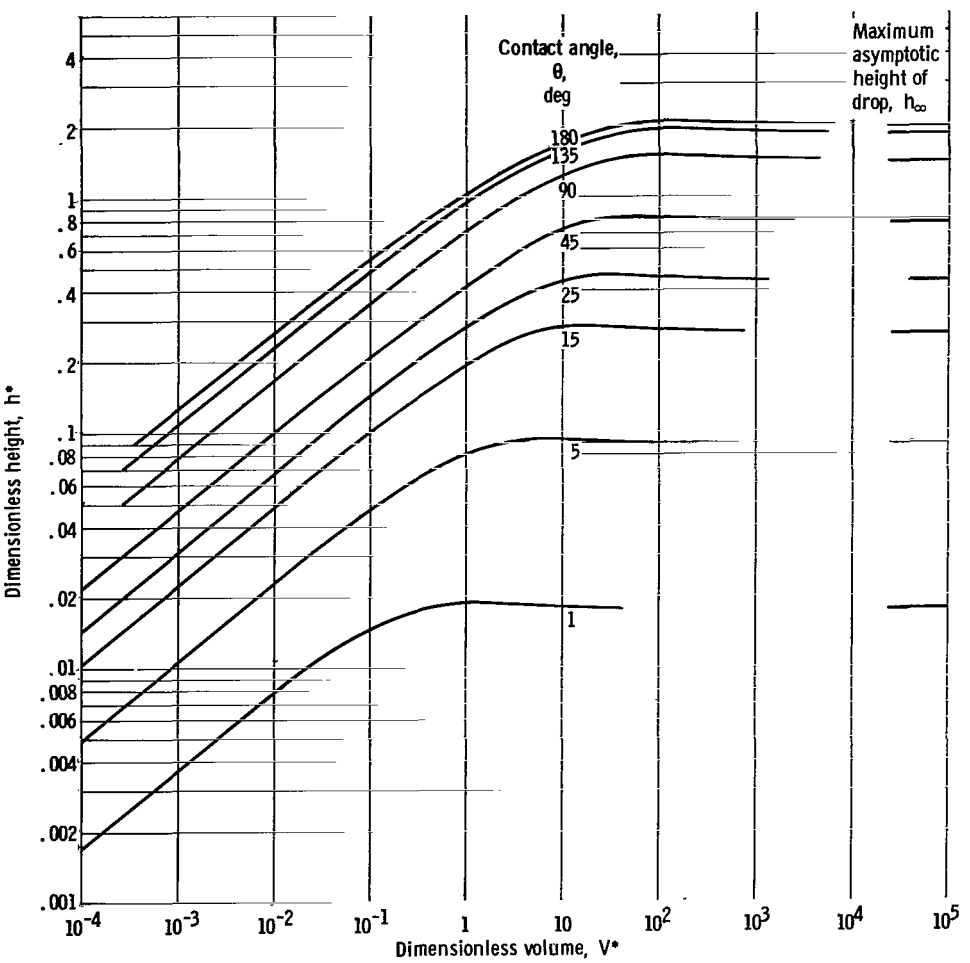

Figure 5. - Dimensionless drop height as function of contact angle.

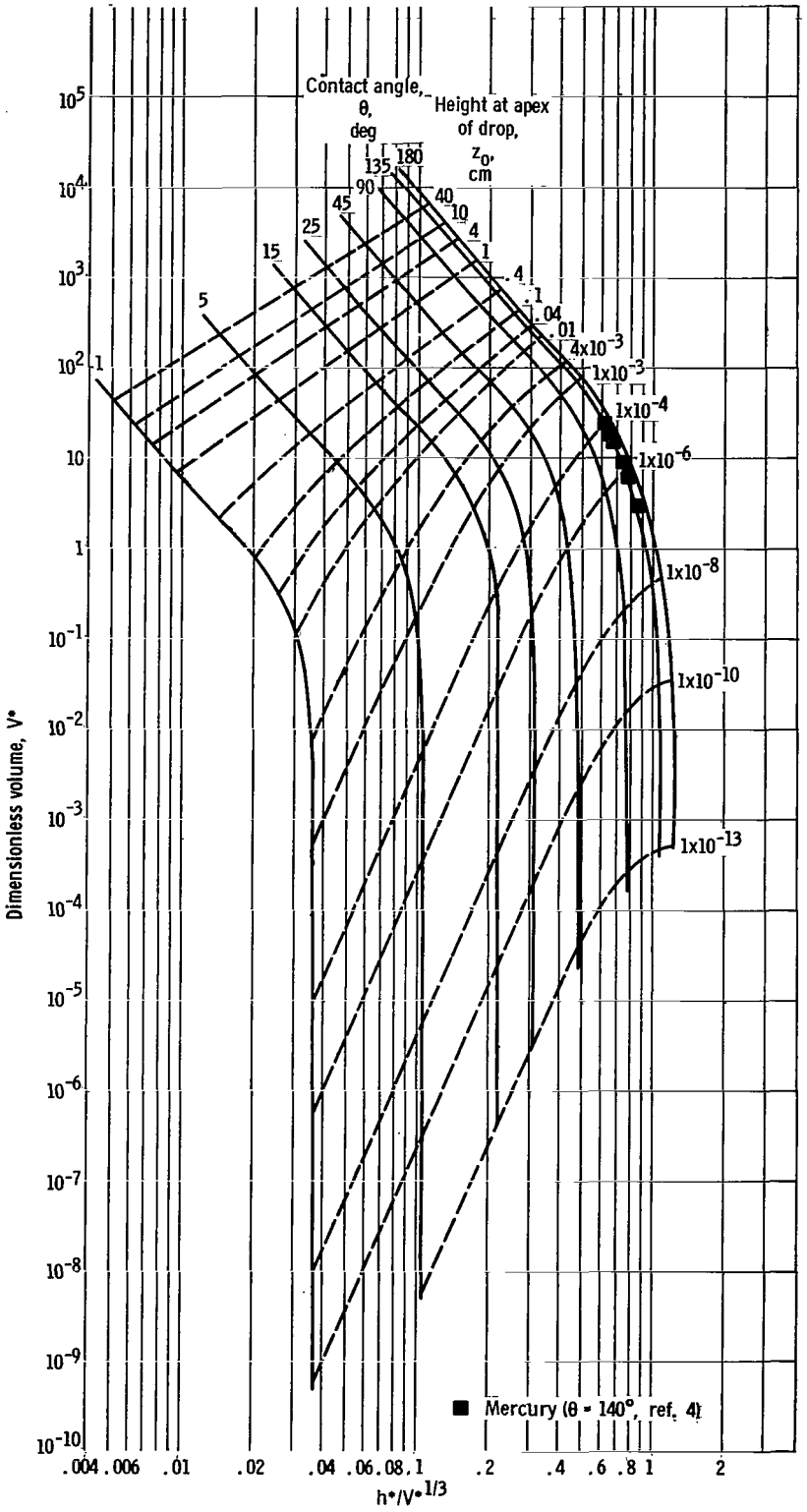

Figure 6. - $h^*/V^{*1/3}$ as function of volume of drop for various contact angles.

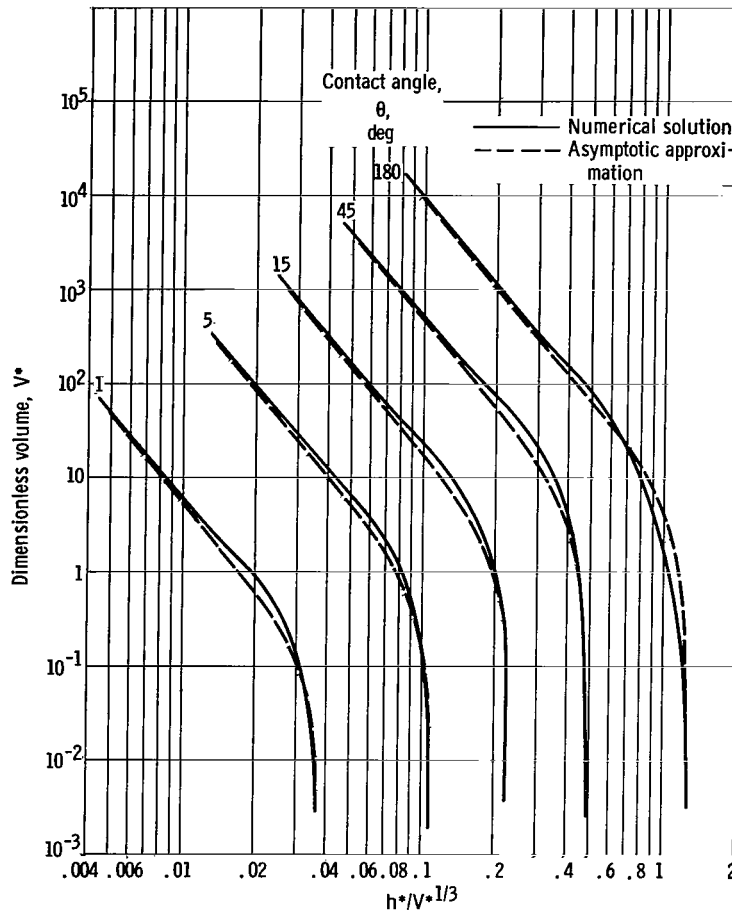

Figure 7. - Comparison of numerical and approximate solutions for $h^*/V^{*1/3}$ as function of dimensionless volume for various contact angles.

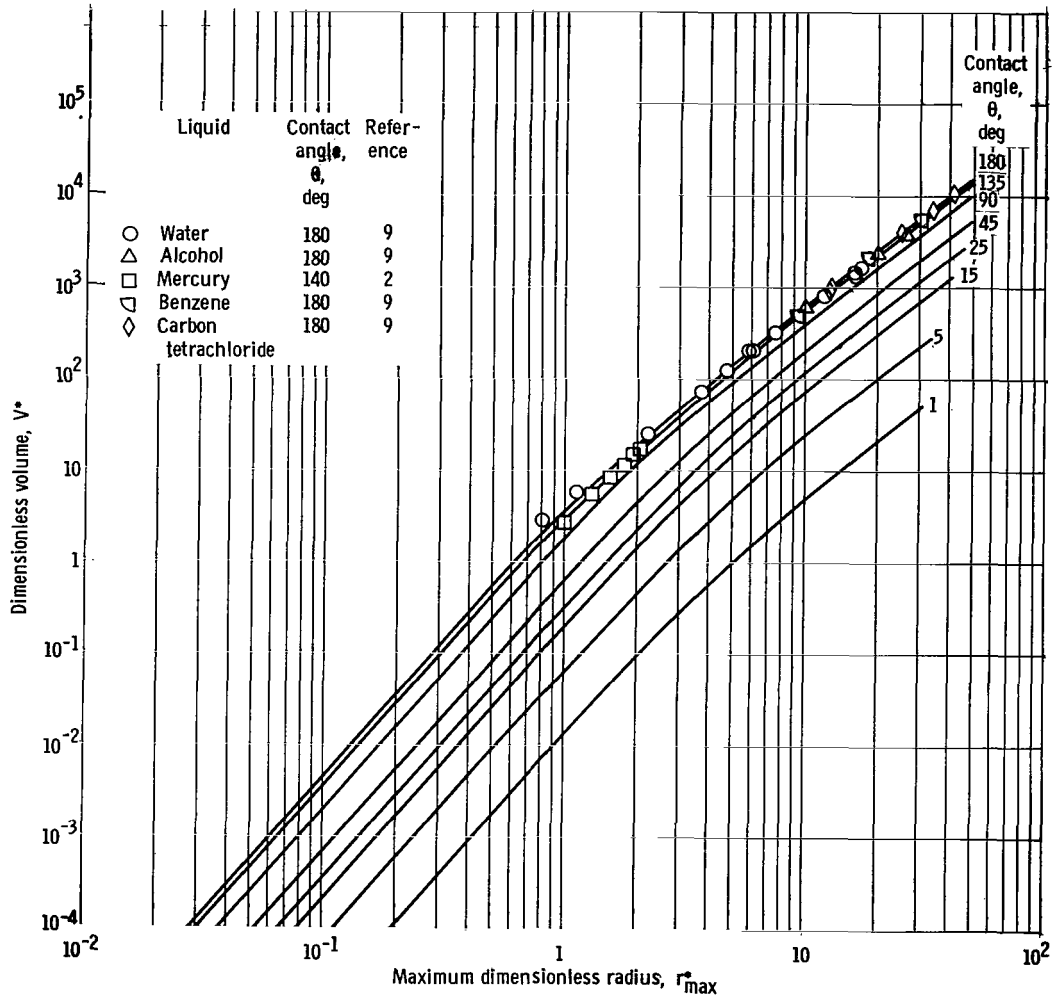

Figure 8. - Maximum drop radius as function of volume of drop and contact angle.

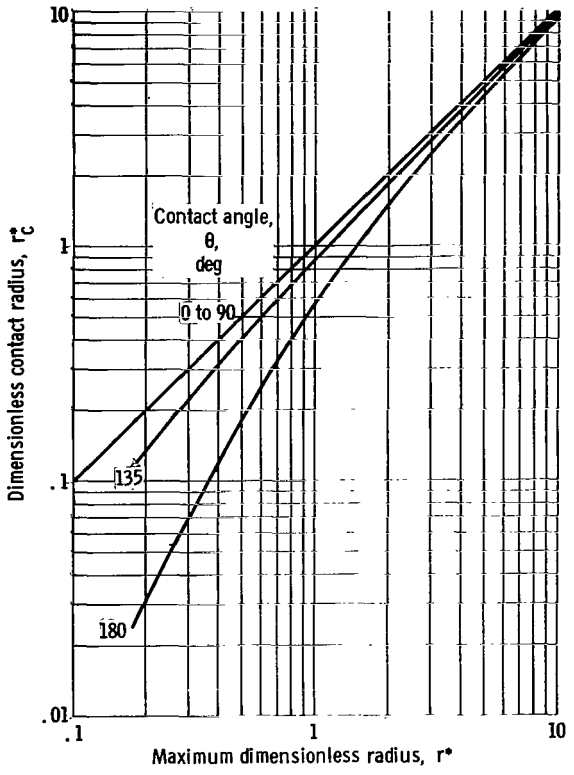

Figure 9. - Relation between contact and maximum drop radius.

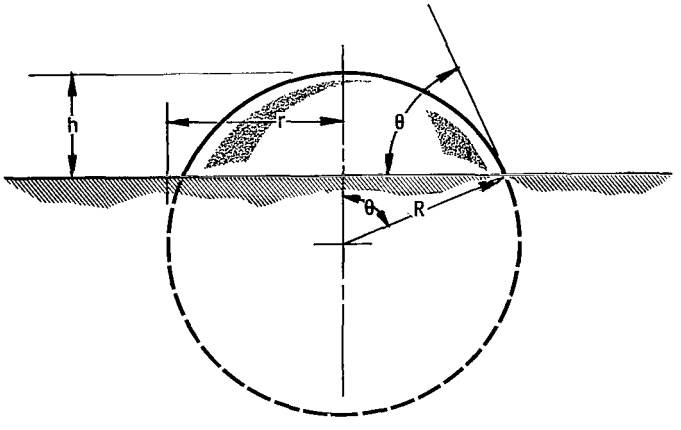

Figure 10. - Spherical drop.

NASA-Langley, 1968 —— 12 E-3329

NATIONAL AERONAUTICS AND SPACE ADMINISTRATION
WASHINGTON, D. C. 20546

OFFICIAL BUSINESS

FIRST CLASS MAIL

POSTAGE AND FEES PAID
NATIONAL AERONAUTICS AND
SPACE ADMINISTRATION

"The aeronautical and space activities of the United States shall be conducted so as to contribute . . . to the expansion of human knowledge of phenomena in the atmosphere and space. The Administration shall provide for the widest practicable and appropriate dissemination of information concerning its activities and the results thereof."

—NATIONAL AERONAUTICS AND SPACE ACT OF 1958

NASA SCIENTIFIC AND TECHNICAL PUBLICATIONS

TECHNICAL REPORTS: Scientific and technical information considered important, complete, and a lasting contribution to existing knowledge.

TECHNICAL NOTES: Information less broad in scope but nevertheless of importance as a contribution to existing knowledge.

TECHNICAL MEMORANDUMS: Information receiving limited distribution because of preliminary data, security classification, or other reasons.

CONTRACTOR REPORTS: Scientific and technical information generated under a NASA contract or grant and considered an important contribution to existing knowledge.

TECHNICAL TRANSLATIONS: Information published in a foreign language considered to merit NASA distribution in English.

SPECIAL PUBLICATIONS: Information derived from or of value to NASA activities. Publications include conference proceedings, monographs, data compilations, handbooks, sourcebooks, and special bibliographies.

TECHNOLOGY UTILIZATION PUBLICATIONS: Information on technology used by NASA that may be of particular interest in commercial and other non-aerospace applications. Publications include Tech Briefs, Technology Utilization Reports and Notes, and Technology Surveys.

Details on the availability of these publications may be obtained from:

SCIENTIFIC AND TECHNICAL INFORMATION DIVISION

NATIONAL AERONAUTICS AND SPACE ADMINISTRATION

Washington, D.C. 20546